



## King's Research Portal

DOI:

[10.1093/europace/euz165](https://doi.org/10.1093/europace/euz165)

*Document Version*

Peer reviewed version

[Link to publication record in King's Research Portal](#)

*Citation for published version (APA):*

Mukherjee, R. K., Mendonca Costa, C., Neji, R., Harrison, J. L., Sim, I. J. W., Williams, S. E., Whitaker, J., Chubb, M. H., O'Neill, L. J., Schneider, R., Lloyd, T., Pohl, T., Roujol, S., Niederer, S. A., Razavi, R., & O'Neill, M. (2019). Evaluation of a real-time magnetic resonance imaging-guided electrophysiology system for structural and electrophysiological ventricular tachycardia substrate assessment. *Europace*, 21(9), 1432-1441. <https://doi.org/10.1093/europace/euz165>

### **Citing this paper**

Please note that where the full-text provided on King's Research Portal is the Author Accepted Manuscript or Post-Print version this may differ from the final Published version. If citing, it is advised that you check and use the publisher's definitive version for pagination, volume/issue, and date of publication details. And where the final published version is provided on the Research Portal, if citing you are again advised to check the publisher's website for any subsequent corrections.

### **General rights**

Copyright and moral rights for the publications made accessible in the Research Portal are retained by the authors and/or other copyright owners and it is a condition of accessing publications that users recognize and abide by the legal requirements associated with these rights.

- Users may download and print one copy of any publication from the Research Portal for the purpose of private study or research.
- You may not further distribute the material or use it for any profit-making activity or commercial gain
- You may freely distribute the URL identifying the publication in the Research Portal

### **Take down policy**

If you believe that this document breaches copyright please contact [librarypure@kcl.ac.uk](mailto:librarypure@kcl.ac.uk) providing details, and we will remove access to the work immediately and investigate your claim.

1 **Evaluation of a real-time MRI-guided electrophysiology**  
2 **system for structural and electrophysiological**  
3 **ventricular tachycardia substrate assessment**

---

4  
5 *Mukherjee et al. Real-time MRI-guided electrophysiology*

6

7 **Full author list:**

8 Rahul K. Mukherjee, MBBS<sup>1</sup>

9 Caroline Mendonca Costa, PhD<sup>1</sup>

10 Radhouene Neji, PhD<sup>1,3</sup>

11 James L. Harrison, BM BCh, PhD<sup>1,2</sup>

12 Iain Sim, MBBS<sup>1</sup>

13 Steven E. Williams MB ChB, PhD<sup>1,4</sup>

14 John Whitaker BM BCh, PhD<sup>1</sup>

15 Henry Chubb, MBBS, PhD<sup>1</sup>

16 Louisa O'Neill, MB BCh<sup>1</sup>

17 Rainer Schneider, PhD<sup>5</sup>

18 Tom Lloyd, MS<sup>6</sup>

19 Thomas Pohl, PhD<sup>5</sup>

20 Sébastien Roujol, PhD<sup>1</sup>

21 Steven A. Niederer, DPhil<sup>1</sup>

22 Reza Razavi, MD<sup>1</sup>

23 Mark D. O'Neill, MB BCh, DPhil, FHRS<sup>1,4</sup>

24 **Affiliations:**

25 <sup>1</sup> School of Biomedical Engineering and Imaging Sciences, 4<sup>th</sup> Floor, North Wing, King's  
26 College London, United Kingdom, SE1 7EH

27

28 <sup>2</sup> Department of Cardiology, King's College Hospital NHS Foundation Trust, London,  
29 United Kingdom

30

31 <sup>3</sup> Siemens Healthcare, Frimley, United Kingdom

32

33 <sup>4</sup> Department of Cardiology, Guy's and St Thomas' NHS Foundation Trust, London, United  
34 Kingdom, SE1 7EH

35

36 <sup>5</sup> Siemens Healthcare GmbH, Erlangen, Germany

37

38 <sup>6</sup> Imricor Medical Systems, Burnsville, MN, United States of America

39

40

41

42 **Address for correspondence:** Dr. Rahul Mukherjee, Division of Imaging Sciences and

43 Biomedical Engineering, King's College London, 4<sup>th</sup> Floor North Wing, St. Thomas'

44 Hospital, London, SE1 7EH. Email: [rahul.r.mukherjee@kcl.ac.uk](mailto:rahul.r.mukherjee@kcl.ac.uk). Tel: 02071885440, Fax:

45 02078483182

46

47 **Word count** - 3481

48 **Conflict of interest** - RN, RS and TP are employees of Siemens Healthcare and receive

49 salary support. TL is an employee of Imricor Medical Systems and receives salary support.

50 The remaining authors have no relevant conflicts of interest to declare.

51

52

53

54

55

56

57

58

59

60

61

62

**63 Condensed abstract**

64

65 A real-time MRI-guided electrophysiology (MR-EP) system was used to assess structural and

66 electrophysiological substrate in a porcine ischaemia-reperfusion model. There was a

67 moderate correlation between regions of low voltage and delayed conduction identified using

68 the MR-EP system and late gadolinium enhancement (LGE).

69

70

71

72

73

74

75

76

77

78

79

80

81

82

83

84

85

86

87

88

89

90

91

92

93

94

95

96

97

98

99

100

101

102

103

104

105

106

107 **What's new?**

- 108       • Endocardial voltage mapping and limited assessments of slow conduction were  
109       feasible in a porcine ischaemia-reperfusion model using a novel real-time MRI-  
110       guided electrophysiology system (MR-EP)
- 111       • Using conventional bipolar voltage thresholds, there was moderate sensitivity in the  
112       ability of voltage mapping with the MR-EP system to identify regions of late  
113       gadolinium enhancement (LGE)
- 114       • An improved sensitivity for LGE detection may be achieved using higher normal  
115       bipolar voltage cut-offs with the MR-EP system and respective MR-compatible  
116       catheter

117

118

119

120

121

122

123

124

125

126

127

128

129

130

131

132 Abstract:

133 **Background:**

134 Potential advantages of real-time magnetic resonance imaging-guided electrophysiology  
135 (MR-EP) include contemporaneous 3D substrate assessment at the time of intervention,  
136 improved procedural guidance and ablation lesion assessment.

137

138 **Objective:**

139 We evaluated a novel real-time MR-EP system to perform endocardial voltage mapping and  
140 assessment of delayed conduction in a porcine ischaemia-reperfusion model.

141

142 **Methods**

143 Sites of low voltage and slow conduction identified using the system were registered and  
144 compared to regions of late gadolinium enhancement (LGE) on MRI. The Sorensen-Dice  
145 similarity coefficient (DSC) between LGE scar maps and voltage maps was computed on a  
146 nodal basis.

147

148 **Results**

149 A total of 445 electrograms were recorded in sinus rhythm (range: 30-186) using the MR-EP  
150 system including 138 electrograms from LGE regions. Pacing captured at 103 sites; 47  
151 (45.6%) sites had a stimulus-to-QRS (S-QRS) delay of  $\geq 40$ ms. Using conventional (0.5mV-  
152 1.5mV) bipolar voltage thresholds, the sensitivity and specificity of voltage mapping using  
153 the MR-EP system to identify MR-derived LGE was 57% and 96% respectively. Voltage  
154 mapping had a better predictive ability in detecting LGE compared to S-QRS measurements  
155 using this system (area under curve: 0.907 vs 0.840). Using an electrical threshold of 1.5mV  
156 to define abnormal myocardium, the total DSC, scar DSC and normal myocardium DSC

157 between voltage maps and LGE scar maps was  $79.0\% \pm 6.0\%$ ,  $35.0\% \pm 10.1\%$  and  $90.4\% \pm$   
158  $8.6\%$  respectively.

159

160 **Conclusions:**

161 Low voltage zones and regions of delayed conduction determined using a real-time MR-EP  
162 system are moderately associated with LGE areas identified on MRI.

163

164 **Keywords:**

165 Real-time, magnetic resonance imaging, electroanatomic mapping, substrate, ventricular  
166 tachycardia, late gadolinium enhancement

167

168 Abstract word count - 237

169

170

171

172

173

174

175

176

177

178

179

180

181

182

183

184

185

186

187

188

189

190

191

## 192 **Introduction**

193 There is growing interest in the use of real-time magnetic resonance imaging-guided  
194 electrophysiology (MR-EP) to treat patients with cardiac arrhythmias.<sup>1,2</sup> Potential advantages  
195 of MR-EP procedures include soft tissue visualisation with a high contrast-to-noise ratio,  
196 improved assessment of arrhythmia structural substrate using late gadolinium enhancement  
197 (LGE) scar imaging, navigation of catheters using dedicated tracking techniques, online  
198 monitoring of ablation lesion formation and an evaluation of anatomic and physiologic  
199 changes during mapping and lesion delivery.<sup>3</sup>

200

201 Although most preliminary real-time MR-EP studies have been performed in the atria, where  
202 significant technical challenges remain for accurate substrate evaluation,<sup>1,2,4</sup> MRI is the gold  
203 standard imaging modality for assessment of ventricular function and scar burden.<sup>5</sup>

204 Combined MR-EP techniques could offer synergistic benefits for the evaluation and ablation  
205 of ventricular tachycardia (VT) substrate. Previous studies using conventional systems and  
206 image integration where the association between electrical substrate for VT and MRI-derived  
207 scar have been investigated invariably report registration errors on a scale between 3.8 -  
208 4.3mm<sup>6,7</sup> which could be a significant source of mis-match.<sup>8</sup> Real-time MR-EP enables  
209 image registration to be performed within a single imaging modality, acquire imaging and  
210 electrical data in the same coordinate system and minimise translational changes due to beat-  
211 to-beat cardiac motion and respiratory motion.

212

213 In this study, we describe the ability of a novel real-time MR-EP system to perform  
214 endocardial voltage mapping and limited assessments of delayed conduction in a porcine  
215 ischaemia-reperfusion model taking advantage of custom technical developments in a second  
216 generation MR-compatible catheter and a dedicated prototype image-guidance platform for



217 interventional procedures. We hypothesised that with the minimisation of registration errors  
218 and translational changes expected using a real-time MR-EP platform, an improved  
219 association between structural and electrophysiological substrate may be expected.

220

## 221 **Methods**

### 222 *Animal model and infarct preparation:*

223

224 The research protocol was approved by the local institutional review board and complied  
225 with French law on animal experiments and the Guiding Principles for the Care and Use of  
226 Laboratory Animals published by the National Institutes of Health (8th Edition, National  
227 Academies Press, 2011). The research was performed at the Institut de Chirurgie Guidée par  
228 l'image (IHU), Strasbourg, France. Seven male domestic pigs (weight -  $35.7 \pm 5\text{kg}$ ; 2  
229 healthy, 5 post infarction) were treated with 800mg amiodarone, twice daily for 4 days prior  
230 to and following an infarct procedure and/or imaging and electrophysiology studies. A  
231 closed-chest model of myocardial infarction was used as previously described.<sup>9</sup> (See  
232 supplementary data for detailed methods).

233

### 234 *Imaging study*

235

236 All animals underwent a MRI scan for substrate assessment 6 weeks after infarct on a 1.5T  
237 scanner (MAGNETOM, Aera, Siemens Healthcare, Erlangen, Germany). Each animal was  
238 sedated, intubated and mechanically ventilated as per the infarct procedure for all imaging  
239 studies. A 3D ECG-triggered whole heart bSSFP MRI dataset was acquired to enable manual  
240 segmentations of cardiac chambers (transverse slice orientation, AP phase encoding, 256 x  
241 256 in-plane matrix size, TR/TE/ $\alpha$  = 3.7ms/1.64ms/90°, voxel size = 1.25x1.25x2.5mm<sup>3</sup>,

242 bandwidth = 895Hz/Px, GRAPPA factor = 2). For scar imaging, contrast was administered  
243 (Gadovist, Bayer, Germany) at a dose of 0.2mmol/kg. High-resolution 3D late gadolinium  
244 enhancement (LGE) imaging was performed using a free-breathing, respiratory navigator and  
245 ECG-gated (in diastole) inversion recovery, b-SSFP sequence ((TR/TE/ $\alpha$ =3.45ms/1.5ms/90°,  
246 FOV=339×264×100mm<sup>3</sup>, voxel size=1.2×1.2×1.2mm<sup>3</sup>, bandwidth=895Hz/Px, GRAPPA  
247 factor=2, 2RR acquisition). The LGE sequence was run 10-15 minutes after administration of  
248 contrast. Based on the LGE-MRI, scar was manually segmented using a version of the  
249 Medical Imaging Interaction Toolkit (MITK, Heidelberg, Germany) with the full-width-half-  
250 maximum (FWHM) threshold used to define scar and help guide electroanatomic mapping  
251 (EAM) during the subsequent procedure.

252

### 253 *iCMR image guidance platform*

254

255 A custom interventional cardiovascular magnetic resonance (iCMR) image guidance  
256 platform (Siemens Healthcare, Erlangen, Germany) was used in this study (Figures 1 and 2).  
257 The application has the ability to load volumetric data from MRI scans, display multi-plane  
258 reconstructions (MPR) in 3 orthogonal planes and transfer segmentations of cardiac  
259 chambers derived from previous imaging or imaging acquired at the time of the EAM  
260 procedure. An automatic segmentation tool is incorporated within the software to ensure  
261 rapid image processing. During the MR-EP procedure, the MPR slices on the iCMR  
262 application can follow the tip of the actively tracked catheter to display 3D location of the  
263 catheter within the segmentations of the cardiac chambers as well as on the MPR images  
264 (Figure 2). The position of the actively tracked catheter is displayed following the  
265 implementation of a temporal smoothing algorithm that limits its excursion due to cardiac  
266 motion.

267 The software allows the imaging operator to start/stop sequences remote from the scanner  
268 console and configure parameters of each sequence on the MRI scanner. A MR-compatible  
269 foot-switch is also available as part of the application to start or pause an interactive imaging  
270 sequence that the electrophysiologist can operate (e.g. to use MPRs to navigate the catheter to  
271 a region of interest). The mapping interface of the application allows for changes to the  
272 rendering style or colour of a loaded segmentation, as well as place markers in regions of  
273 interest (e.g. to highlight EGMs or mark sites of ablation). The iCMR application  
274 communicates directly with the Advantage EP Recording system to display recorded  
275 activation times and voltage amplitudes. Colour interpolation is used to display this data  
276 which is computed by a relaxation algorithm that takes the values on the mapping points as  
277 the fixed boundary condition and then performs a linear interpolation on the segmentation  
278 surface between these mapping points. These features enable the system to closely mimic that  
279 of a clinical EAM system whilst having additional capabilities to utilise imaging data for  
280 procedure guidance.

281

### 282 *Real-time MRI-guided electrophysiology procedure*

283

284 Vascular access was obtained via the femoral artery and vein under ultrasound guidance (9Fr  
285 or 10Fr introducer sheath) followed by administration of 100 units/kg of intravenous heparin.  
286 All EAM studies were performed inside the MRI scanner without the use of fluoroscopy at  
287 any point. The left ventricle (LV), right ventricle (RV), left atrium (LA), right atrium (RA)  
288 and aorta were manually segmented from the 3D ECG-triggered whole heart bSSFP MRI  
289 dataset using the MITK-based platform. Image processing was performed during a 45-minute  
290 window following the completion of imaging studies and prior to the start of EAM. During  
291 this time, each animal remained inside the scanner in order to minimise translational changes

292 due to subject movement between imaging and mapping. The 3D shells of each chamber  
293 were imported into the iCMR guidance platform and displayed using the 3D-whole heart  
294 dataset to act as a 'road-map' for mapping studies. The 3D segmentation of scar from the  
295 LGE-MRI was also imported into the iCMR guidance platform and overlaid onto the 3D  
296 shell for the LV chamber.

297

298 A custom 9Fr, MR-compatible steerable catheter with a single gold 3.5mm tip and ring  
299 bipolar electrode (3.5mm inter-electrode spacing) and six circumferential open irrigation  
300 ports (Vision-MR, Imricor, Burnsville, MN, USA) was advanced into the LV cavity via  
301 retrograde aortic access. A number of modifications were implemented to the MR-compatible  
302 catheter from previous versions used in the atria<sup>1,2</sup> to enable manipulation in the left ventricle  
303 (Supplementary Data). These changes enabled improved torque transfer within the ventricle,  
304 manoeuvrability and consistency of shape following deflection. The MR-compatible catheter  
305 has 2 solenoid micro-coils located 2mm and 11mm proximal to the ring electrode that  
306 enabled the location and orientation of the catheter to be detected in 3D space using a  
307 dedicated MRI active tracking sequence. A custom-built MR-EP recording system  
308 (Advantage-MR, Imricor, Burnsville, MN, USA) consisting of a digital amplifier, stimulator  
309 and host workstation was used to record, display and analyse intra-cardiac electrograms as  
310 previously described.<sup>10</sup> A patient monitoring system suitable for use in the MRI environment  
311 (Invivo, Gainesville, Florida) was used to monitor a single lead ECG and invasive arterial  
312 blood pressure throughout the study.

313

314

315 *Active catheter tracking of MR-compatible catheter*

316

317 In order to accurately detect the location and orientation of the mapping catheter in 3D space,  
318 a dedicated active tracking sequence was used as described previously.<sup>10</sup> Briefly, the X, Y, Z  
319 coordinates of the catheter micro-coils were determined using the custom active tracking  
320 sequence, which was optionally interleaved with a fast balanced steady state free precession  
321 (bSSFP) imaging sequence automatically following the current catheter position. The active  
322 tracking sequence comprised three non-selective projection acquisitions along the respective  
323 axis. A dynamic imaging coil detuning approach and pre-spoiler were applied to avoid  
324 potential background noise, i.e. coil coupling and residual signal effects. Based on the  
325 acquired projections, the corresponding signal peaks were detected with a dynamic template-  
326 matching algorithm, which used the initial projections to calculate a template per coil and  
327 axis. The template was continuously updated with each new projection fulfilling a minimal  
328 peak-to-noise ratio to adapt to the changing shape of the projections while manoeuvring the  
329 catheter. The detected positions were fed back to both the iCMR platform (Siemens  
330 Healthcare) and the MRI scanner to update the rendered catheter position/orientation and  
331 imaging plane location respectively.<sup>10</sup>

332

### 333 *Intra-cardiac Electrogram recording and characterisation*

334

335 Activation and voltage data were acquired during sinus rhythm. For each sampling point, the  
336 time delay (LAT) from a fixed intra-cardiac reference point to the initial deflection of the  
337 local LV electrogram was measured manually on the EP recording system and data  
338 transferred to the iCMR image guidance platform. Similarly, the peak-to-peak voltage  
339 amplitude was also measured manually and transmitted to the guidance platform (Figure 1).  
340 Both datasets were used to generate colour-coded activation and voltage maps on the iCMR  
341 platform. Areas of focused mapping were based on the location of LGE-derived scar. In order

342 to avoid EGM artifacts due to poor catheter-tissue contact, at least 2 consecutive EGMs had  
343 to have the same morphology prior to acceptance of each mapping point. Regions of  
344 abnormal myocardium were defined as areas with a bipolar voltage threshold  $<1.5\text{mV}$ .<sup>11</sup>  
345 EGMs were reviewed off-line at a sweep speed of 100mm/s. After acquisition of activation  
346 and voltage maps, the LV catheter was used to pace during stable sinus rhythm (10mA, 3ms,  
347 cycle length 10% shorter than sinus cycle length) from sites of normal myocardium and scar.  
348 The time from the stimulus artefact to the surface QRS onset was used to distinguish regions  
349 of normal and delayed conduction. Following confirmation of capture, the time duration  
350 between the stimulus artefact to QRS onset was recorded. The MR-compatible catheter was  
351 sequentially manoeuvred to sites within normal myocardium and scar using active catheter  
352 tracking to generate a colour-coded map of stimulus-QRS duration times (S-QRS). Sites with  
353 a S-QRS  $>40\text{ms}$  during pace-mapping in sinus rhythm were considered regions of slow  
354 conduction as previously described.<sup>12</sup> Following completion of the MR-EP procedure, pigs  
355 were euthanised with potassium chloride and hearts were rapidly dissected for gross  
356 pathological examination. Hearts were photographed with areas of ischaemic scar delineated.

357

### 358 *Image registration, scar segmentation and comparison to voltage maps*

359

360 The LGE-MRI imaging was registered to the 3D whole heart MRI datasets using a point-  
361 based (landmark) rigid registration to guide EAM. Points were selected within the RV, LV  
362 and LA blood pools of each image dataset. Registration was performed on the Medical  
363 Imaging Interaction Toolkit (MITK) [<https://doi.org/10.1016/j.media.2005.04.005>]. Scar was  
364 segmented on the LGE-MRI using the FWHM method to normalise signal intensity relative  
365 to maximum myocardial signal intensity. First, the LV wall was manually segmented using a  
366 custom version of MITK. This was performed using the 'Paint Tool' on the MITK-based

367 platform to derive the endocardial and epicardial border on a slice-by-slice basis with 3D  
368 interpolation to minimise discontinuities between slices. Then, the maximum signal intensity  
369 within the LV wall was computed and the voxels with signal intensity above 50% of the  
370 maximum intensity (FWHM) were labelled as scar.

371

372 To compare the scar segmentation with regions of low voltage, the scar segmentation was  
373 mapped onto the voltage map surface mesh. This was achieved in two steps. First, the scar  
374 segmentation image was rotated and translated so that it was aligned with the surface mesh.  
375 Second, the scar points were mapped onto the surface mesh using the iterative closest point  
376 (ICP) method. In addition, the voltage map was converted to a binary map of scar (1) and  
377 normal tissue (0). In this ischaemia-reperfusion model, scar has been noted to be transmural  
378 in the majority of myocardial segments with LGE.<sup>9</sup> The Sorensen-Dice similarity coefficient  
379 (DSC) between the two binary maps was then computed on a nodal basis for all regions, scar  
380 regions only and regions of normal myocardium. The DSC between LGE scar maps and  
381 voltage maps following thresholding at different cut-offs (0.5mV-3.5mV) was also derived.

382

### 383 *Statistical analysis*

384

385 Data analysis was performed using GraphPad Prism version 7.0 (GraphPad Software, CA,  
386 USA) or SPSS v24.0 (IBM Corp. Armonk, NY, USA). Continuous data are represented as  
387 mean  $\pm$  SD and compared using the Student's two-tailed T-test. A 2-sided p value  $<0.05$  was  
388 considered statistically significant. For assessment of the accuracy of the MR-EP system to  
389 correctly identify scar and delayed conduction, the location of LGE-derived scar was taken as  
390 the 'gold standard' of structural substrate. The sensitivity, specificity, positive predictive  
391 value and negative predictive value of low voltage points and S-QRS times using the MR-EP

392 system to identify LGE-scar was assessed and used to derive receiver operator characteristic  
393 (ROC) curves.

394

## 395 **Results**

396 All pigs that underwent a LAD infarct developed antero-septal scar which was visualised on  
397 the LGE images (mean scar volume -  $6.80 \pm 0.88\text{ml}$ ) - Supplementary data. There was no  
398 LGE present in healthy pigs that did not undergo the LAD infarct procedure.

399

### 400 *Real-time MRI-guided electroanatomical mapping*

401

402 Segmentations of scar from the LGE-MRI were displayed on the iCMR image-guidance  
403 platform as coloured shells to guide EAM (Figure 2). 445 EGMs (range 30-186) were  
404 recorded from all animals in sinus rhythm (including 138 EGMs from regions located within  
405 the LGE scar segmentation). Using the MRI-derived LGE segmentation to differentiate  
406 between normal myocardium and scar, the mean signal-to-noise ratio (SNR) of EGMs within  
407 normal tissue and scar was  $44.78 \pm 21.91$  and  $11.67 \pm 6.99$  respectively ( $p < 0.0001$ ) (Figure  
408 3). Pacing captured at 103 sites whilst 10 sites which were all in regions of LGE-derived scar  
409 did not capture; 56 (54.4%) sites had S-QRS delay  $\leq 40\text{ms}$ , 47 (45.6%) sites had a delay of  
410  $\geq 40\text{ms}$  whilst 15 (14.5%) had a delay  $\geq 80\text{ms}$ . Representative examples of voltage and S-QRS  
411 maps obtained using the system are shown in Figure 4.

412

### 413 *Relationship between MRI-derived scar, voltage and delayed conduction*

414

415 Using conventional (0.5mV-1.5mV) bipolar voltage thresholds, the sensitivity and specificity  
416 of voltage mapping using the MR-EP system to identify MR-derived LGE was 57% and 96%



417 respectively (ROC area under curve = 0.907;  $p < 0.0001$ ). A S-QRS threshold of  $>40$ ms using  
418 this system resulted in a sensitivity of 76% and specificity of 73% to identify MR-derived  
419 LGE (ROC area under curve = 0.840;  $p < 0.0001$ ) - Figure 5. At a threshold of 1.5mV to  
420 define abnormal myocardium, the positive predictive value (PPV) and negative predictive  
421 value (NPV) of voltage mapping to identify LGE was 86% and 83% respectively. At a  
422 threshold of 40ms, the PPV and NPV of S-QRS time using the system to identify LGE was  
423 73% and 79% respectively (Figure 5).

424

425 There was a moderate relationship between low voltage regions in the LV endocardium and  
426 LGE-derived scar mapped onto the endocardial surface mesh (Figure 6). At a voltage  
427 threshold of 1.5mV, mean DSC across all nodes was  $79.0\% \pm 6.0\%$ , whilst mean DSC within  
428 scar regions only was  $35.0\% \pm 10.1\%$  and  $90.4\% \pm 8.6\%$  in normal myocardium regions  
429 only. An improvement in DSC within scar regions was observed using a higher voltage cut-  
430 off of 2.0mV and 2.5mV ( $47.3 \pm 9.9\%$  and  $60.2 \pm 22.4\%$ ) at the expense of reduced  
431 agreement across regions of normal myocardium (Figure 7).

432

### 433 **Discussion**

434

435 This study shows that the prototype real-time MR-EP system can be used to guide catheters  
436 to regions of scar using active catheter tracking and to distinguish regions of low voltage and  
437 delayed conduction from healthy myocardium. There is a moderate relationship between low  
438 voltage and LGE scar using conventional bipolar voltage thresholds. An improved sensitivity  
439 for LGE detection may be achieved using higher bipolar voltage cut-offs with this system.

440

441 The relationship between local EGM amplitude and scar is complex, in part due to the  
442 dependence of voltage on infarct size, heterogeneity and transmural. <sup>13</sup> Conventional  
443 bipolar voltage thresholds for scar detection may lack sensitivity to fully detect scar as  
444 variations in inter-electrode spacing and recording electrode size may affect the  
445 representation of EGMs. <sup>11</sup> Furthermore, although LGE-MRI is the current gold standard for  
446 visualisation of ventricular scar post myocardial infarction, the limited spatial resolution of *in*  
447 *vivo* LGE-MRI can result in partial volume effects and limit the specificity of scar  
448 characterisation. <sup>13</sup> Increasing mapping resolution using multi-electrode catheters may also  
449 result in detection of a smaller area of low bipolar voltage as each data point represents a  
450 smaller tissue area with less far-field contamination <sup>14</sup>. The use of multi-electrode catheters  
451 could improve the correlation between EAM and imaging as has been shown in a randomised  
452 study. <sup>15</sup> An additional source of discrepancy when correlating EAM and pre-procedural  
453 imaging is registration error due to translational changes (patient movement, cardiac or  
454 respiratory motion) or changes in volume, orientation or rhythm of the heart between time of  
455 imaging and EAM. <sup>16</sup>

456

457 The real-time MR-EP system minimises registration error through registration of electrical  
458 and structural data within a single imaging modality with the same coordinate system. The  
459 3D whole heart sequence used for chamber segmentation was acquired during the same phase  
460 of the cardiac cycle as the 3D LGE to minimise translational changes due to beat-to-beat  
461 cardiac motion. Furthermore, both sequences were performed when animals were under  
462 general anaesthesia with reduced variability in respiratory motion thereby minimising  
463 translational changes due to respiratory motion. Compared to image integration approaches,  
464 where positional errors are introduced when registering catheter position to pre-procedural  
465 imaging, the MR-EP system tracks catheter position directly using a dedicated tracking

466 sequence that is acquired in the same coordinate system as the 3D whole heart and LGE  
467 scans. The main sources of error with the MR-EP system include within scan registration  
468 error and catheter tip displacement on the 3D shell with the active tracking sequence. In a  
469 cohort of conscious patients scanned with an angiography sequence to create an endocardial  
470 mask and a 3D LGE acquisition, the within scan translation error was noted to be  $1.9 \pm$   
471  $1.6\text{mm}$  with a rotation error of  $0.62 \pm 0.41^\circ$ .<sup>17</sup> This is, however, likely to overestimate within  
472 scar error with the MR-EP system where translational movements were minimal as animals  
473 were under general anaesthesia. Using ex-vivo technical validation, the average tip  
474 displacement of the actively tracked catheter using the MR-EP system was measured as  $0.90$   
475  $\pm 0.58\text{mm}$  along the axis of the catheter<sup>1</sup> and is likely to be the best estimate of error with this  
476 set-up.

477

478 In this study, we show that despite the minimisation of registration and translational errors,  
479 the relationship between scar delineated using a custom MR-compatible catheter and high  
480 resolution isotropic LGE imaging ( $1.2\text{mm}^3$ ) remains moderate when using standard voltage  
481 thresholds. An improvement in scar concordance with this system can be achieved using a  
482 higher normal bipolar voltage cut-off. Some investigators have found that abnormal  
483 potentials targeted for ablation may be present in tissue classified as ‘normal’ ( $>1.5\text{mV}$ )  
484 voltage and manual adjustment of bipolar voltage thresholds to higher cut-off values may  
485 identify more confluent scar regions incorporating all abnormal signals.<sup>18</sup> Regions of slow  
486 conduction could also be present in tissue of normal bipolar voltage and unmasked during  
487 extrastimulus pacing.<sup>19</sup>

488

489 Although the majority of real-time MR-EP studies published previously have focused on the  
490 atria, the full potential of substrate and lesion assessment afforded by such systems is likely

491 to be realised in the context of VT ablation. There are limited data available evaluating real-  
492 time MR-EP systems in the ventricle.<sup>20,21,22</sup> Our study builds on previous work to characterise  
493 the relationship between LGE-derived scar and electrophysiological measurements of low  
494 voltage and delayed conduction inside a MRI scanner.

495

496 Currently, limited visualisation of soft tissue structures is possible in the electrophysiology  
497 laboratory with the use of intra-cardiac ultrasound (ICE), however MRI offers an improved  
498 contrast-to-noise ratio and ability to acquire 3D whole heart images or 2D slices in any  
499 imaging plane. Furthermore, tissue characterisation techniques such as LGE can be used to  
500 identify arrhythmogenic substrate whilst dedicated sequences can be used to monitor tissue  
501 temperature during ablation and provide a real-time method of calculating lethal thermal  
502 dose.<sup>10</sup> The novel MR-EP system described is capable of visualising the location and  
503 orientation of catheters relative to soft tissue, assess scar with MRI at the time of EAM,  
504 enable rapid segmentation and registration of cardiac chambers and potentially monitor  
505 formation of ablation lesions.<sup>10</sup> These features of the MR-EP system could offer an  
506 alternative to conventional fluoroscopy-guided or ICE-guided procedures and improve  
507 catheter navigation, delivery of therapy and assess anatomical and physiological changes  
508 during VT ablation with the potential to reduce risks and improve outcomes.

509

510 A number of technical developments are required prior to the realisation of real-time MRI-  
511 guided VT ablation. The development of a MRI-compatible defibrillation system will be a  
512 prerequisite prior to any clinical studies and prototypes are currently under evaluation.<sup>23</sup>  
513 Current surface ECG monitoring systems inside a MRI scanner are limited to 4-6 surface  
514 electrodes; in order to aid the diagnostic electrophysiology requirements of VT ablation,  
515 robust 12-lead ECG systems are required. Although high-fidelity 12-lead ECG recordings are

516 possible,<sup>24</sup> the impact of magneto-hydrodynamic effects and gradient switching-induced  
517 voltages within the MRI scanner can still corrupt ECG signals. There is currently a limited  
518 availability of MR-compatible devices; the development of MR-compatible multi-electrode  
519 catheters with similar capabilities to their conventional counterparts will accelerate progress  
520 in the electrophysiological assessment of substrate inside the scanner.<sup>25</sup>

521

## 522 **Limitations**

523 There are several important limitations to this study. We did not define the bipolar voltage  
524 threshold that best correlates to histological scar using the MR-compatible catheter - rather  
525 two indirect methods of scar assessment were compared to each other. During assessment of  
526 S-QRS intervals to assess slow conduction, a single ECG lead was used to derive  
527 measurements due to the lack of availability of a MRI-compatible 12-lead ECG; as a result,  
528 no assessment of QRS morphology using a 12-lead ECG was performed during pacing.  
529 These measurements should therefore be interpreted with caution as we could not account for  
530 local latency although this would be expected to be minimal at the pacing cycle length used.  
531 Furthermore, the technique of S-QRS measurements may have limited sensitivity for the  
532 detection of regions of myocardium with slow conduction compared to an approach  
533 analysing the evoked response to extrastimuli.<sup>19</sup> In this model, haemodynamic compromise  
534 and death of the animal was inevitable if VT was induced. As there was no means to  
535 defibrillate the animal inside the scanner, we deliberately avoided the induction of VT which  
536 in turn precluded entrainment mapping. The MR-EP system used in this study consisted of a  
537 single electrode catheter and required manual annotation of activation times and voltages for  
538 each point on the EP recording system resulting in substantially lower mapping densities than  
539 with contemporary EAM systems. This could have lowered the precision of the sensitivity  
540 and specificity measures reported in the study. The development of automated mapping

541 systems and multi-polar catheters for use inside the MRI scanner could better define the  
542 relationship between electrophysiological substrate and MR-derived substrate.

543

#### 544 **Conclusions**

545 There is a moderate association between low voltage regions and sites of altered conduction  
546 determined using a novel real-time MR-EP system with scar derived from LGE-MRI. An  
547 improved sensitivity for LGE detection could be achieved using a higher normal voltage cut-  
548 off with this system and the respective catheter. Further technical developments in MR-  
549 compatible devices will accelerate progress towards real-time MRI-guided VT ablation.

550

#### 551 **Acknowledgements**

552 This work was funded by a Wellcome Trust Health Innovation Challenge Fund grant (HICF-  
553 R10-698). The research was also supported by the Wellcome/EPSRC Centre for Medical  
554 Engineering at King's College London [WT 203148/Z/16/Z] and Department of Health  
555 through a National Institute of Health Research Comprehensive Biomedical Research Centre  
556 award to Guy's and St Thomas' NHS Foundation Trust in partnership with King's College  
557 London and King's College Hospital NHS Foundation Trust. Dr Whitaker is a recipient of a  
558 Fellowship award from the Medical Research Council (MRC CRTF N001877/1). The views  
559 expressed are those of the author(s) and not necessarily those of the NHS, the NIHR, MRC or  
560 the Department of Health.

561

#### 562 **References**

563 <sup>1</sup> Chubb H, Harrison JL, Weiss S, Krueger S, Koken P, Bloch LO et al. Development, pre-  
564 clinical validation and clinical translation of a cardiac magnetic resonance-electrophysiology

565 system with active catheter tracking for ablation of cardiac arrhythmia. Journal of the  
566 American College of Cardiology: Clinical Electrophysiology 2017: 3; 89-103.

567

568 <sup>2</sup> Hilbert S, Sommer P, Gutberlet M, Gaspar T, Foldyna B, Piorkowski C et al. Real-time  
569 magnetic resonance-guided ablation of typical right atrial flutter using a combination of  
570 active catheter tracking and passive catheter visualisation in man: initial results from a  
571 consecutive patient series. Europace 2016: 18; 572-7.

572

573 <sup>3</sup> Mukherjee RK, Whitaker J, Williams SE, Razavi R, O'Neill MD. Magnetic resonance  
574 imaging guidance for the optimization of ventricular tachycardia ablation. Europace 2018:  
575 20; 1721-32.

576

577 <sup>4</sup> Paetsch I, Sommer P, Jahnke C, Hilbert S, Loebe S, Schoene K et al. Clinical workflow and  
578 applicability of electrophysiological cardiovascular magnetic resonance-guided  
579 radiofrequency ablation of isthmus-dependent atrial flutter. European Heart Journal:  
580 Cardiovascular Imaging 2018: October 10. Epub ahead of print.

581

582 <sup>5</sup> Dawson DK, Hawlisch K, Prescott G, Roussin I, Di Pietro E, Deac M, Wong J, Frenneaux  
583 MP, Pennell DJ, Prasad SK. Prognostic role of CMR in patients presenting with ventricular  
584 arrhythmias. Journal of the American College of Cardiology: Cardiovascular Imaging 2013:  
585 6; 335-44.

586

587 <sup>6</sup> Wijnmaalen AP, van der Geest RJ, van Huls van Taxis CFB, Siebelink H-MJ, Kroft LJM,  
588 Bax JJ, Reiber JHC, Schalij MJ, Zeppenfeld K. Head-to-head comparison of contrast-  
589 enhanced magnetic resonance imaging and electroanatomical voltage mapping to assess post-

590 infarct scar characteristics in patients with ventricular tachycardias: real-time image  
591 integration and reversed registration. *European Heart Journal* 2011; 32; 104-114.

592

593 <sup>7</sup> Desjardins B, Crawford T, Good E, Oral H, Chugh A, Pelosi F et al. Infarct architecture and  
594 characteristics on delayed enhanced magnetic resonance imaging and electroanatomic  
595 mapping in patients with postinfarction ventricular arrhythmia. *Heart Rhythm* 2009; 6; 644-  
596 51.

597

598 <sup>8</sup> Roujol S, Basha TA, Khanna V, Chan RH, Moghari MH, Rayatzadeh H et al. Improved  
599 multimodality data fusion of late gadolinium enhancement MRI to left ventricular voltage  
600 maps in ventricular tachycardia ablation. *IEEE Transactions in Biomedical Engineering*  
601 2013; 60; 1308-17.

602

603 <sup>9</sup> Tschabrunn CM, Roujol S, Nezafat R, Faulkner-Jones B, Buxton AE, Josephson ME, Anter  
604 E. A swine model of infarct-related re-entrant ventricular tachycardia: electroanatomic,  
605 magnetic resonance and histopathological characterization. *Heart Rhythm* 2016; 13; 262-73.

606

607 <sup>10</sup> Mukherjee RK, Roujol S, Chubb H et al. Epicardial electroanatomical mapping,  
608 radiofrequency ablation and lesion imaging in the porcine left ventricle under real-time  
609 magnetic resonance imaging guidance - an in-vivo feasibility study. *Europace* 2018; 20: 254-  
610 262.

611

612 <sup>11</sup> Tung R, Kim S, Yagishita D, Vaseghi M, Ennis DB, Ouadah S, Ajjola OA, Bradfield JS,  
613 Mahapatra S, Finn P, Shivkumar K. Scar voltage threshold determination using ex vivo  
614 magnetic resonance imaging integration in a porcine infarct model: influence of



615 interelectrode distances and three-dimensional spatial effects of scar. Heart Rhythm 2016; 13;  
616 1993-2002.

617

618 <sup>12</sup> Brunckhorst CB, Stevenson WG, Soejima K, Maisel WH, Delacretaz E, Friedman PL,  
619 Ben-Haim SA. Relationship of slow conduction detected by pace-mapping to ventricular  
620 tachycardia re-entry circuit sites after infarction. Journal of the American College of  
621 Cardiology 2003; 41; 802-9.

622

623 <sup>13</sup> Lopez-Yunta M, Leon DG, Alfonso-Almazan JM, Marina-Breyse M, Quintanilla JG,  
624 Sanchez-Gonzalez J et al. Implications of bipolar voltage mapping and magnetic resonance  
625 imaging resolution in biventricular scar characterisation after myocardial infarction.  
626 Europace 2019; 21; 163-74.

627

628 <sup>14</sup> Tschabrunn CM, Roujol S, Dorman NC, Nezafat R, Josephson ME, Anter E. High-  
629 resolution mapping of ventricular scar: comparison between single and multi-electrode  
630 catheters. Circulation: Arrhythmia and Electrophysiology 2016; 9; e003841.

631

632 <sup>15</sup> Acosta J, Penela D, Andreu D, Cabrera M, Carlosena A, Vassanelli F et al. Multielectrode  
633 vs. point-by-point mapping for ventricular tachycardia substrate ablation: a randomized  
634 study. Europace 2018; 20: 512-19.

635

636 <sup>16</sup> Roujol S, Anter E, Josephson ME, Nezafat R. Characterisation of respiratory and cardiac  
637 motion from electroanatomical mapping data for improved fusion of MRI to left ventricular  
638 electrograms. PLoS One 2013; 8; e78852.

639

640 <sup>17</sup> Chubb H, Karim R, Roujol S, Nunez-Garcia M, Williams SE, Whitaker J et al. The  
641 reproducibility of late gadolinium enhancement cardiovascular magnetic resonance imaging  
642 of post-ablation atrial scar: a cross-over study. *Journal of Cardiovascular Magnetic  
643 Resonance* 2018; 20; 21.

644

645 <sup>18</sup> Jais P, Maury P, Khairy P, Sacher F, Nault I, Komatsu Y et al. Elimination of local  
646 abnormal ventricular activities: a new end point for substrate modification in patients with  
647 scar-related ventricular tachycardia. *Circulation* 2012; 125; 2184-96.

648

649 <sup>19</sup> Acosta J, Andreu D, Penela D, Cabrera M, Carlosena A, Korshunov V et al. Elucidation of  
650 hidden slow conduction by double ventricular extrastimuli: a method for further arrhythmic  
651 substrate identification in ventricular tachycardia ablation procedures. *Europace* 2018; 20;  
652 337-46.

653

654 <sup>20</sup> Nazarian S, Kolandaivelu A, Zviman MM, Meiningner GR, Kato R, Susil RC, Roguin A,  
655 Dickfeld TL, Ashikaga H, Calkins H, Berger RD, Bluemke DA, Lardo AC, Halperin HR.  
656 Feasibility of real-time magnetic resonance imaging for catheter guidance in  
657 electrophysiology studies. *Circulation* 2008; 118; 223-9.

658

659 <sup>21</sup> Oduneye SO, Pop M, Biswas L, Ghate S, Flor R, Ramanan V, Barry J, Celik H, Crystal E,  
660 Wright GA. Post-infarction ventricular tachycardia substrate characterisation: a comparison  
661 between late enhancement magnetic resonance imaging and voltage mapping using a MR-  
662 guided electrophysiology system. *IEEE Transactions in Biomedical Engineering* 2013; 60;  
663 2442-9.

664

665 <sup>22</sup> Oduneye SO, Pop M, Shurrab M, Biswas L, Ramanan V, Barry J, Crystal E, Wright GA.  
666 Distribution of abnormal potentials in chronic myocardial infarction using a real-time  
667 magnetic resonance guided electrophysiology system. *Journal of Cardiovascular Magnetic*  
668 *Resonance* 2015; 17;27.

669

670 <sup>23</sup> Schmidt EJ, Watkins RD, Zviman MM, Guttman MA, Wang W, Halperin HA. A magnetic  
671 resonance imaging-conditional external cardiac defibrillator for resuscitation within the  
672 magnetic resonance imaging scanner bore. *Circulation: Cardiovascular Imaging* 2016; 9;  
673 e005091.

674

675 <sup>24</sup> Tse ZT, Dumoulin CL, Clifford GD, Schweitzer J, Qin L, Oster J, Jerosch-Herold M,  
676 Kwong RY, Michaud G, Stevenson WG, Schmidt EJ. A 1.5T MRI-conditional 12-lead  
677 electrocardiogram for MRI and intra-MR intervention. *Magnetic Resonance in Medicine*  
678 2014; 71; 1336-47.

679

680 <sup>25</sup> Elbes D, Magat J, Govari A, Ephrath Y, Vieillot D, Beeckler C, Weerasooriya R, Jais P,  
681 Quesson B. Magnetic resonance imaging-compatible circular mapping catheter: an in vivo  
682 feasibility and safety study. *Europace* 2017; 19; 458-64.

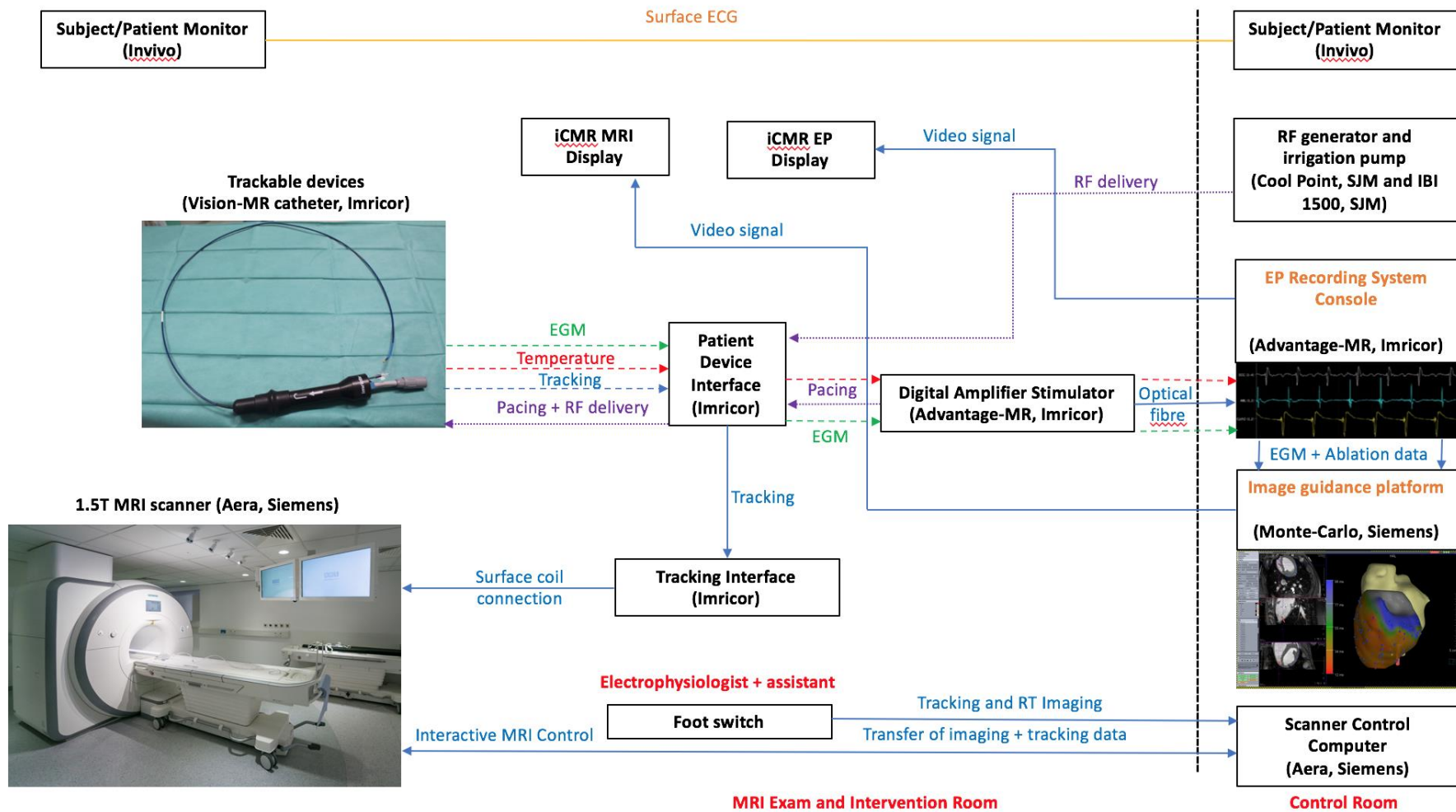


**Figure 1:** Set-up of the real-time MR-EP system to enable electrophysiology studies inside a MRI scanner.

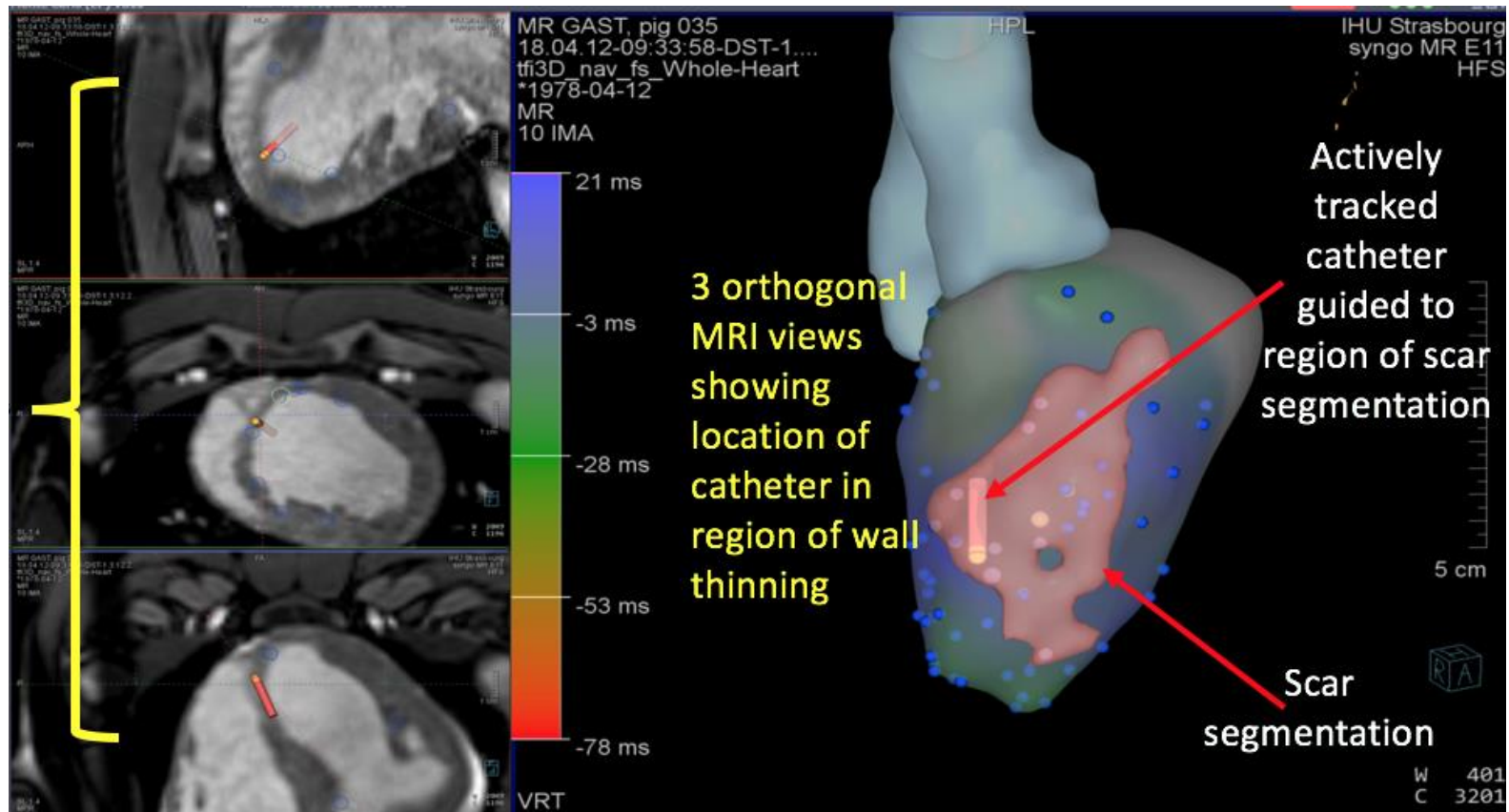


**Figure 2:** Representative depiction of image guidance platform showing 3 orthogonal MRI views demonstrating location of catheter in relation to LV endocardium, 3D segmentation of the left ventricle derived from MRI and scar segmentation from LGE images to guide EAM.

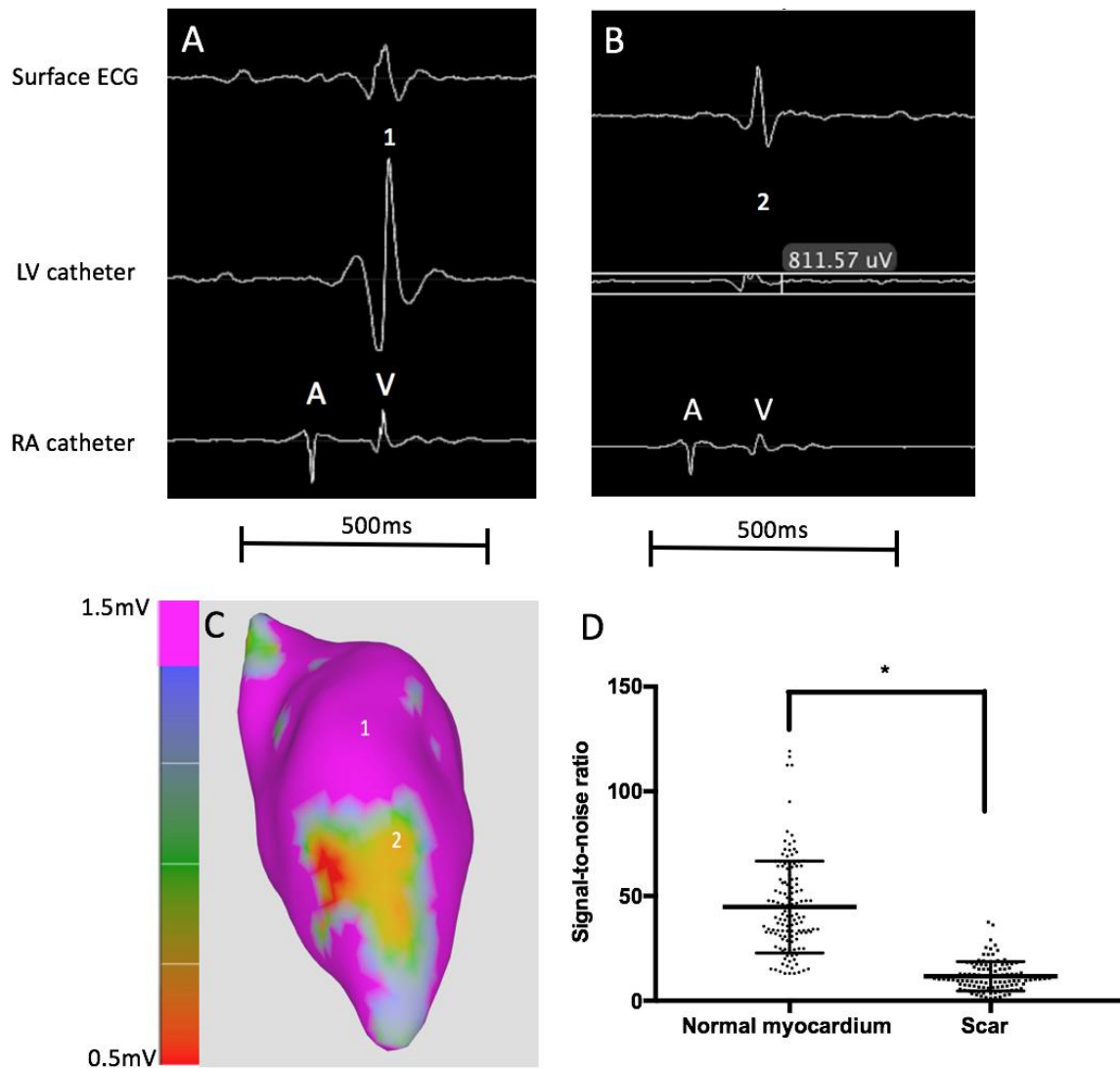


**Figure 3:** Representative examples of intra-cardiac EGMs obtained using the MR-EP system in a region of normal myocardium (Point 1) and area of scar (Point 2) (A-C). The baseline noise level inside the MRI scanner was in the region of 0.1mV (approximately 10-fold higher than that in the conventional electrophysiology laboratory). Dot-plot showing signal-to-noise ratios obtained for intra-cardiac EGMs in normal myocardium and LGE-derived scar regions from 7 animals; \* $p < 0.0001$  (D).

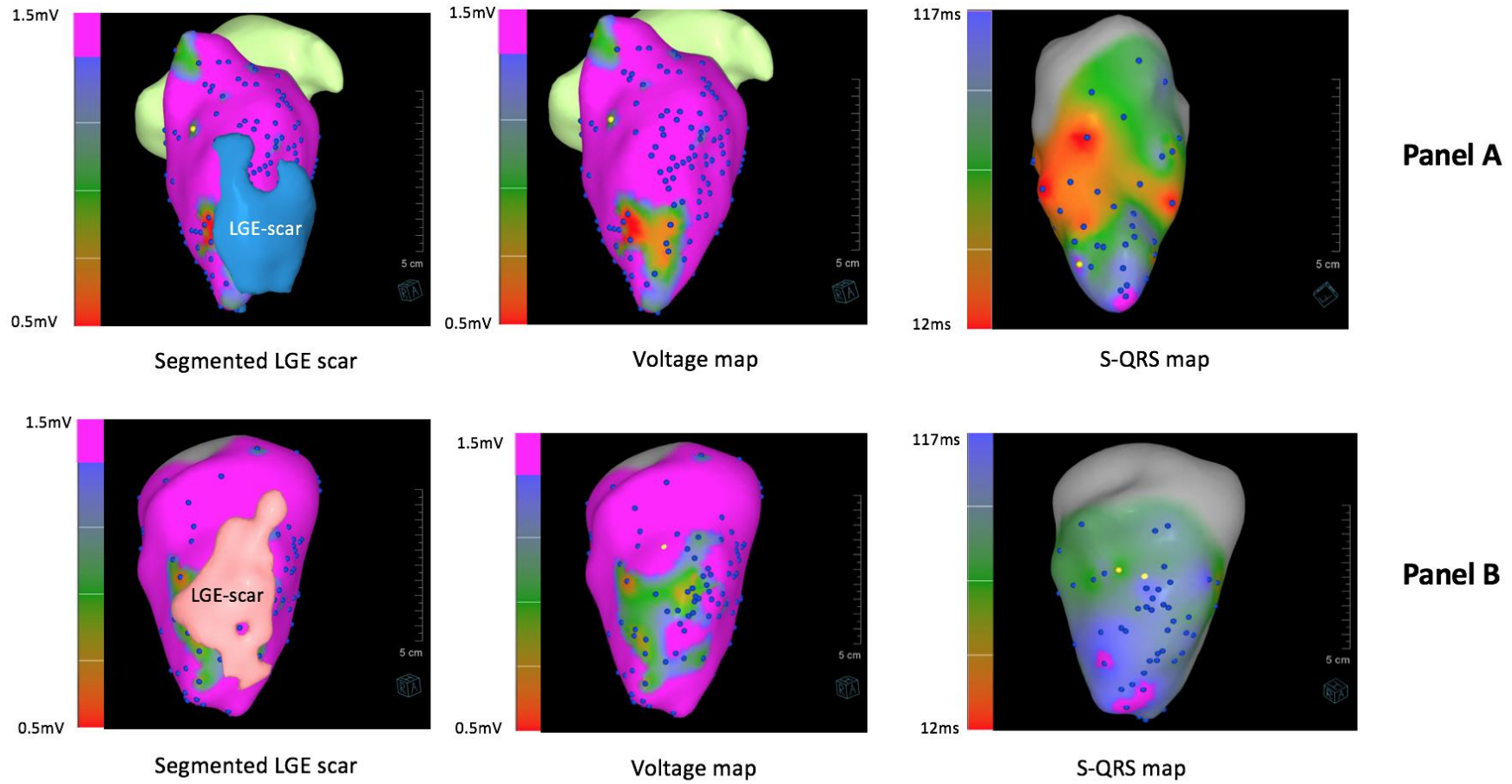


**Figure 4:** Representative examples of segmented LGE scar, voltage and S-QRS maps obtained using real-time MR-EP system in 2 animals (Panel A and B)

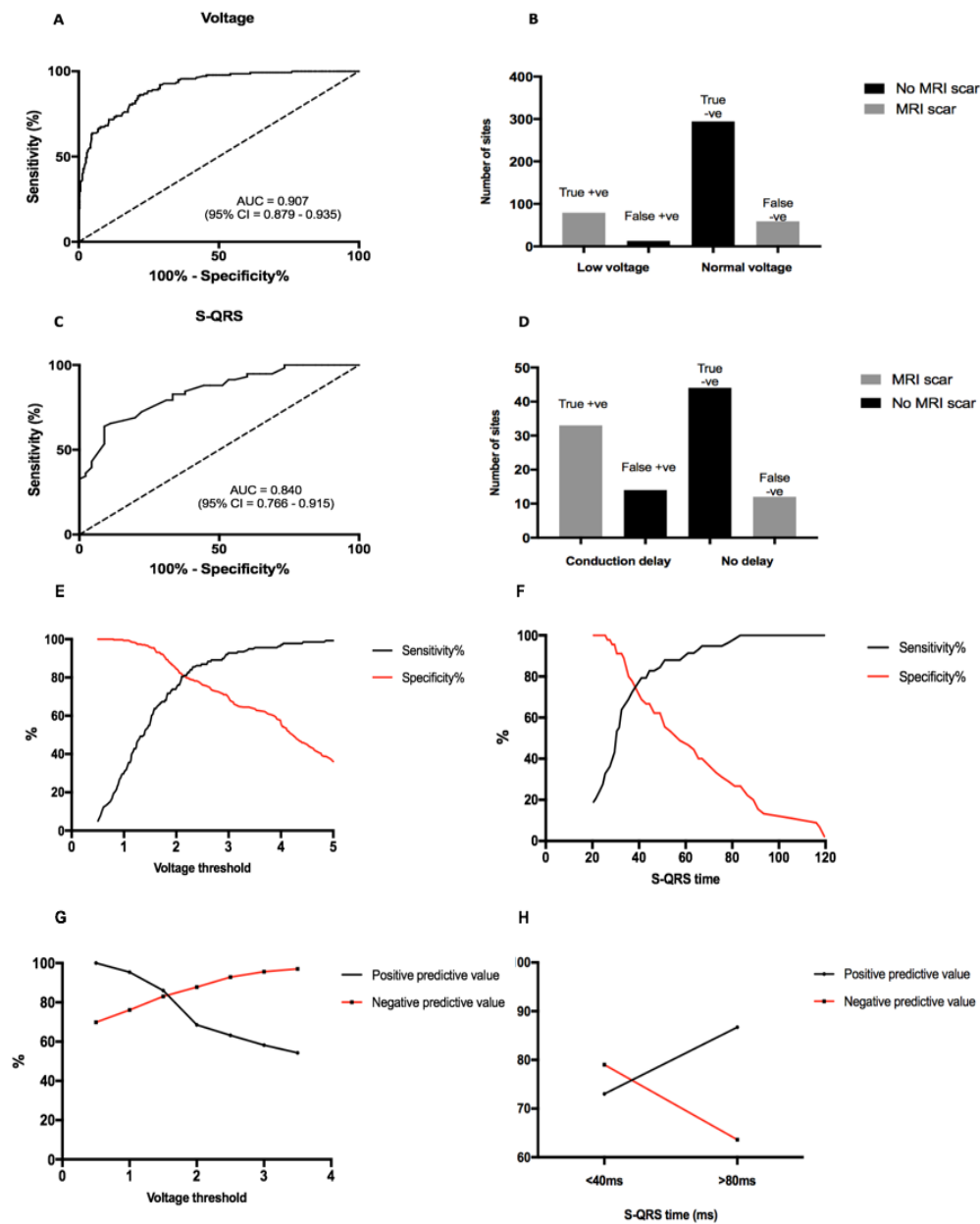


**Figure 5:** ROC curves (A and C) for prediction of LGE regions using voltage mapping and S-QRS. Frequency histograms (B and D) displaying the true positive, false positive, true negative and false negative counts of voltage mapping and S-QRS measurements using the real-time MR-EP system to predict MRI-derived scar. Sensitivity, specificity, PPV and NPV of measurements using the system using different normal voltage cut-offs and S-QRS times (E-H)



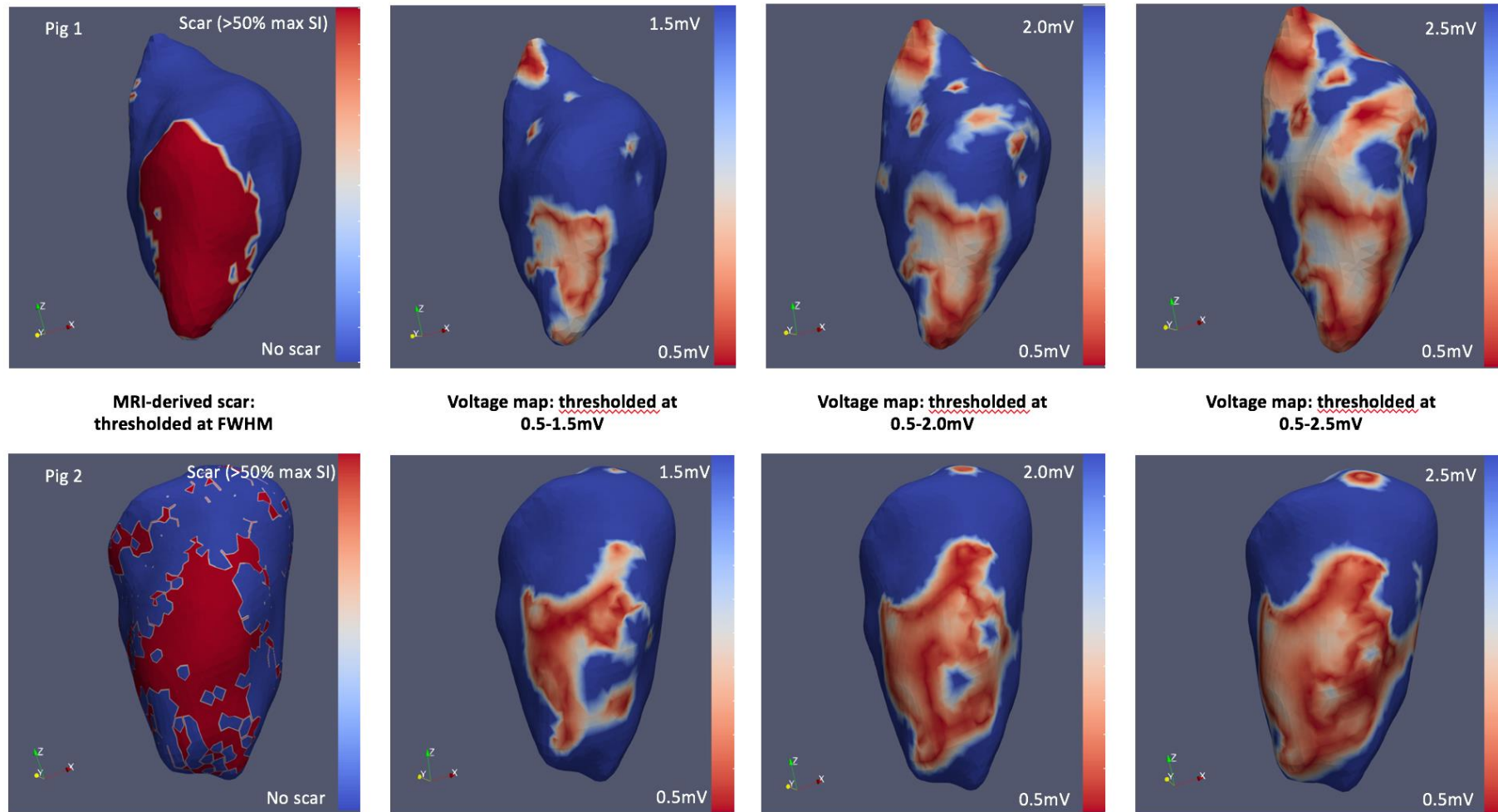


**Figure 6:** Sorenson-Dice similarity co-efficient between MR-derived scar shells (far left panels) and endocardial voltage maps with varying normal voltage thresholds (right panels) in 2 representative animals.

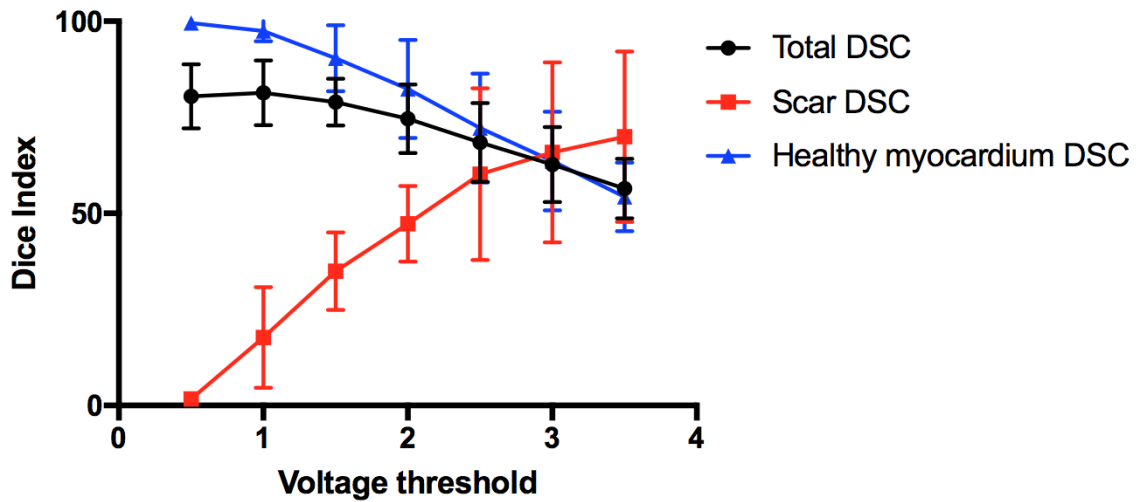


**Figure 7:** Dice similarity co-efficients (DSC) between MR-derived scar shells and endocardial voltage maps acquired using MR-EP system following application of normal cut-off thresholds of 0.5-3.5mV. DSC is shown for overall similarity, similarity across scar nodes and normal myocardium nodes.



